

Relationship Between Properties Degradation and Critical Aging Time of Super Austenitic and Duplex Stainless Steels

S. H. Choi¹, Y. R. Yoo^{2†}, S. Y. Won¹, G. B. Kim¹, and Y. S. Kim^{1, 2†}

¹Department of Materials Science and Engineering, Andong National University,
1375 Gyeongdong-ro, Andong, Gyeongbuk, 36729, South Korea

²Materials Research Centre for Energy and Clean Technology, Andong National University,
1375 Gyeongdong-ro, Andong, Gyeongbuk, 36729, South Korea

(Received October 14, 2023; Revised October 23, 2023; Accepted October 24, 2023)

The objective of this study was to analyze effects of aging time on property degradation of super austenitic stainless steel of PRE 52.8 and super duplex stainless steel of PRE 48.7. To analyze corrosion properties based on aging time, a critical pitting temperature test was performed in a solution of 6% FeCl₃ + 1% HCl and an anodic polarization test was performed in deaerated 0.5N HCl + 1N NaCl solution at a temperature of 50 °C. Surface hardness was measured to analyze mechanical properties. It was found that corrosion properties and mechanical properties deteriorated rapidly as aging time increased. Critical pitting temperature had the most effect on critical aging time at which property changes occurred rapidly, followed by pitting potential and hardness. This trend was found to be closely related to the fraction of sigma phase. Rate of sigma phase formation was found to be significantly faster in duplex stainless steel than in austenitic stainless steel.

Keywords: Critical aging time, CPT, Pitting potential, Hardness, Sigma fraction

1. Introduction

Stainless steels are widely used in various industries due to their excellent corrosion resistance, high temperature performance, and excellent mechanical properties [1-4]. Stainless steels have a wide range of chemical compositions and can be categorized into different microstructures based on their composition, including austenitic, ferritic, duplex, martensitic, and precipitation hardening [5]. The corrosion resistance of stainless steel can be improved by alloying, which can be predicted by the Pitting Resistance Equivalent ($PRE = \%Cr + 3.3\%(Mo + 0.5\%W) + 16\%N$). Stainless steel with a PRE_{16} index of 30 or more can be used in coastal areas, and if the PRE_{16} index is 40 or more, it can be used in high corrosion environments such as nuclear power plants and desulfurization facilities, and these stainless steels are called super stainless steels. However, while the addition of large amounts of alloying elements can improve

corrosion resistance, it can also have other disadvantages. The microstructure of stainless steels can change due to heat treatment, welding processes, and long-term use at high temperatures, leading to changes in their properties [6-8]. The main precipitated phases in stainless steel are sigma (σ), chi (χ), and secondary austenitic phases, and carbides or nitrides of the $M_{23}C_6$ type [9-11]. These precipitation phases appear at a certain temperature, and among them, sigma phase is the most undesirable phase, which is known as the precipitation phase with high content of Cr and Mo. On the other hand, it is known that the diffusion rate of Cr and Mo is faster in ferrite than in austenite [12,13]. Different types of stainless steels have different precipitation mechanisms, which leads to differences in precipitation time.

The precipitation time of the sigma phase was different in duplex stainless steels, ferritic and austenitic stainless steels [14]. In austenitic stainless steels, sigma was initially generated in the grain boundaries, followed by sigma within the grains [15-19]. In ferritic stainless steels, the sigma phase initially precipitated in the grain boundaries, followed quickly by sigma inside the grains [20-23]. In duplex stainless steels, phase transformation

†Corresponding author: yryoo@anu.ac.kr, yikim@anu.ac.kr
S.H. Choi: Ph.D. Candidate, Y.R. Yoo: Senior Researcher, S. Y. Won: M.S. Student, G.B. Kim: M.S. Student, Y.S. Kim: Professor

occurs preferentially within the ferrite, resulting in the precipitation of sigma and a second austenite phase, followed by the precipitation of sigma at the austenite grain boundaries [24-28]. On the other hand, for corrosion properties, all corrosion properties deteriorated with increasing aging time at a certain temperature for all types of stainless steels [29-32]. As for the mechanical properties, the hardness increased due to precipitation strengthening, but the tensile strength decreased significantly [23,33].

Previous studies have investigated the microstructural changes of various precipitation phases in stainless steel and the resulting changes in mechanical properties and corrosion characteristics, but there is a lack of research on the relationship between the amount of sigma phase and aging time. Therefore, in this paper, super austenitic stainless steels and duplex stainless steels were subjected to aging heat treatment at 850 °C to analyze the relationship between changes in degradation properties and critical aging time.

2. Experimental methods

2.1 Specimen preparation

Specimen fabrication involved using a high-frequency induction furnace (capacity 40 kW), into which electrolytic iron, Ni, Mo, W, and Cr were introduced, forming a melt. Following this, Mn, Si, and Co were added, and once all alloy elements were sufficiently melted, deoxidation was performed. Subsequently, Fe-Cr-N was wrapped in aluminum foil and introduced into the melt in 3-4 separate additions. After that, 10 kg of ingot was produced by casting into a ceramic mold measuring 200 × 150 × 20T mm at a temperature of 1,580 °C, and 6 mm of plate was produced by hot rolling.

Table 1 shows the composition of the two experimental alloys (A29 and D27Co) and the pitting resistance

equivalent and sigma formation index of the specimens. The alloys were annealed at 1,125 °C and 1,150 °C for 15 minutes and then quenched. The aging heat treatment was performed at 850 °C. For A29 specimens, an austenitic stainless steel, the aging heat treatment times were 0, 5, 30, 60, 300, 600, 1,500, and 3,000 minutes, and for D27Co specimens, a duplex stainless steel, the aging heat treatment times were 0, 4, 5, 20, 30, 60, and 600 minutes for each alloy type.

2.2 CPT measurement

The measurement of the critical pitting temperature was performed according to the ASTM G48 standard [36]. The specimen entire surface with 1.5 × 1.5 cm², was polished up to #600 with SiC paper, cleaned, and the surface area and weight were measured before testing. The test solution was 6% FeCl₃ + 1% HCl, and pitting tests were conducted at a constant temperature for 24 hours. If the weight loss was below the criterion, the temperature of the solution was increased by 5 °C, and the test was repeated to determine the critical pitting temperature for each specimen.

2.3 Polarization test

The specimens were cut to a size of 1.5 × 1.5 cm², spot welded with insulated sheathed copper wire, and mounted with epoxy resin. One side of the specimen was then polished to SiC paper #600, and the rest of the specimen was insulated with epoxy resin to expose 1 cm² of surface. A potentiostat (Interface 1000, Gamry Instruments, Warminster, PA, USA) was used and a saturated calomel electrode for the reference electrode and Pt wire for the counter electrode were used. The test solution was 0.5 N HCl + 1 N NaCl at 50 °C and deaerated at a rate of 200 mL N₂/min for 30 min. After submersion of the sample into the Avesta cell, cathodic polarization was conducted at a potential of -200 mV from the open circuit potential for a duration of 10 minutes to eliminate surface oxides.

Table 1. Chemical composition of the experimental alloys (wt%)

Alloys	Cr	Mo	W	Si	Ni	Mn	C	N	Co	P	S	Fe	PRE	SFI
A29	28.5	4.0	0.20	0.76	26.3	0.76	0.021	0.36	-	0.002	0.010	Bal.	52.8	42.0
D27Co	27.8	1.9	0.32	0.57	9.4	0.69	0.030	0.47	2.47	0.012	0.006	Bal.	48.7	34.6

* PRE (Pitting Resistance Equivalent) = %Cr + 3.3(%Mo + 0.5%W) + 30%N[34],

* SFI (Sigma Formation Index) = %Cr + 3.3(%Mo + 0.5%W) [35]

Subsequently, it was held at the open circuit potential for an additional 10 minutes. The corrosion potential was then recorded, followed by obtaining the polarization curve, starting from -200 mV relative to the corrosion potential, with a scanning rate of 0.33 mV/s.

2.4 Hardness measurement

Hardness was measured using a Rockwell hardness tester (MRK-M2, MATSUZAWA SEIKI, Japan). One side of the specimen was polished up to SiC paper #120, and hardness was measured on the C-scale. A total of nine measurements were conducted, and the average hardness was calculated using the remaining measurements after excluding the maximum and minimum values.

2.5 Optical microscopic observation

Specimens for microstructure observation were cut to 1.5×1.5 cm², ground up to SiC paper #2000, and polished using a 3 μ m diamond paste. The austenitic stainless steel A29 specimens were etched using an electrolytic etcher (Lectropol 5, Struers, Denmark) in a 10% oxalic acid solution, while the duplex stainless steel D27Co specimens were etched using Murakami's reagent ($K_3Fe(CN)_6$ + KOH + Distilled water) at 50 °C. Finally, the specimens were cleaned in ethyl alcohol using an ultrasonic cleaner, and the microstructures were observed using an optical microscope (AXIOTECH 100HD, ZEISS, Oberkochen, Germany).

2.6 X-ray diffraction analysis

To analyze the structure of precipitated phases, XRD testing was conducted using an Ultima IV (Rigaku, Tokyo, Japan). The specimens were polished to #2000 using SiC paper with both sides horizontal. The scan angle, 2θ , was measured from 30° to 80° and the scan speed was 4° /min.

2.7 SEM-EBSD analysis

The specimens were polished using SiC paper #2000 and a 1 μ m diamond paste. After polishing, ion milling (IM4000, Hitachi, Tokyo, Japan) was performed for 30 minutes. The equipment used for EBSD measurements was an electron backscatter diffractometer (EBSD, Oxford Instruments, Bognor, Regis, UK) attached to a FE-SEM (MIRA3 XMH, Tescan, Brno, Czech Republic) to observe the tissue. The EBSD has a step size of 0.3 μ m. Data for analysis were post-processed using HKL Channel 5 (Oxford Ins., Abingdon, UK) analysis software.

3. Results

3.1 Effect of aging time on the corrosion properties of austenitic and duplex stainless steels

To investigate the changes in the corrosion properties of austenitic stainless steel A29 and duplex stainless steel D27Co, CPT tests (test solution: 6% $FeCl_3$ + 1% HCl) were performed as a function of aging time, and the results are shown in Fig. 1. As shown in the figure, the effect of aging time on the critical equilibrium temperature varies

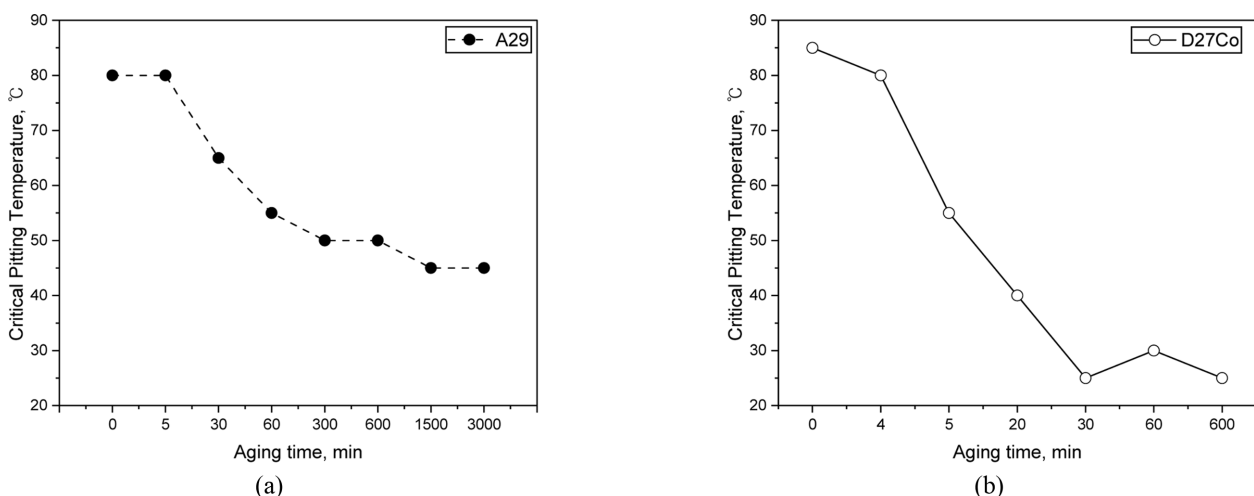


Fig. 1. Effect of aging time on the critical pitting temperature in 6% $FeCl_3$ + 1% HCl: (a) Austenitic A29 alloy and (b) Duplex D27Co alloy

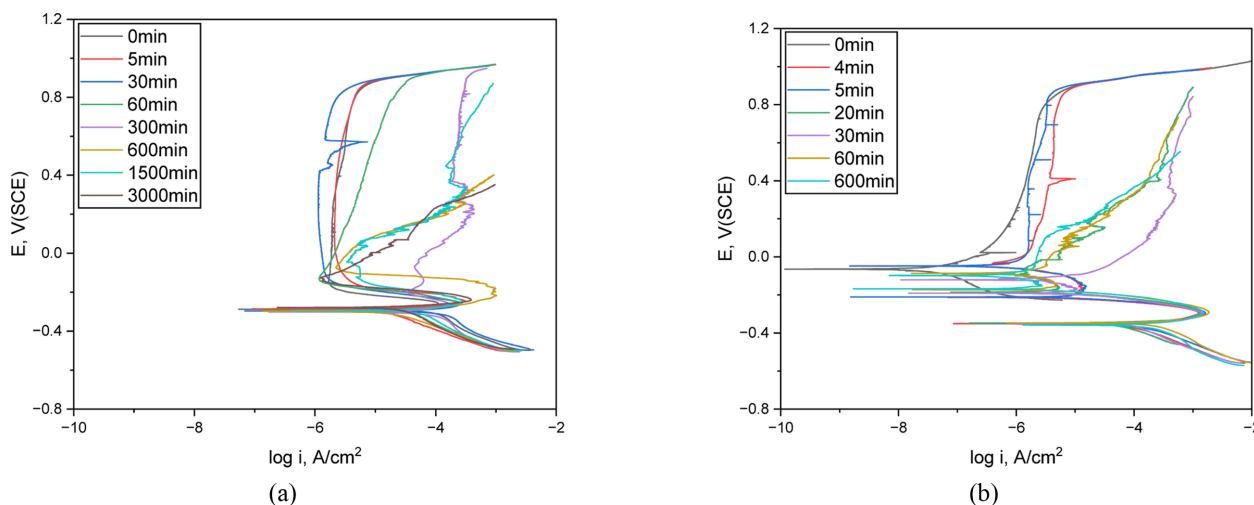


Fig. 2. Effect of aging time on the polarization behavior in deaerated 0.5N HCl + 1N NaCl solution at 50 °C: (a) Austenitic A29 alloy and (b) Duplex D27Co alloy

depending on the alloy. A29, an austenitic stainless steel, showed a decrease in the critical equilibrium temperature at an aging time of 60 minutes, while D27Co, a duplex stainless steel, showed a sharp decrease in the critical equilibrium temperature at 5 minutes. After 1,500 minutes of aging time for A29 and 30 minutes of aging time for D27Co, there was little change in the critical pitting temperature.

Fig. 2 shows the effect of aging time on the polarization behavior in deaerated 0.5 N HCl + 1 N NaCl solution at 50 °C. Fig. 2a shows the results for A29, when the aging time increased, the passivation area decreased and the passivation current density increased, and when the aging

time was 300 min, the pitting potential decreased sharply. Fig. 2b shows the results for D27Co, with increasing aging time, the passivation area decreased and the passivation current density increased, and with an aging time of 20 minutes, the pitting potential dropped rapidly. In addition, a cathodic loop was observed in D27Co at potentials ranging from -0.4 to -0.2 V(SCE).

3.2 Effect of aging time on the surface hardness of austenitic and duplex stainless steels

To investigate the changes in the mechanical properties of A29, an austenitic stainless steel, and D27Co, a duplex stainless steel, the hardness was measured as a function

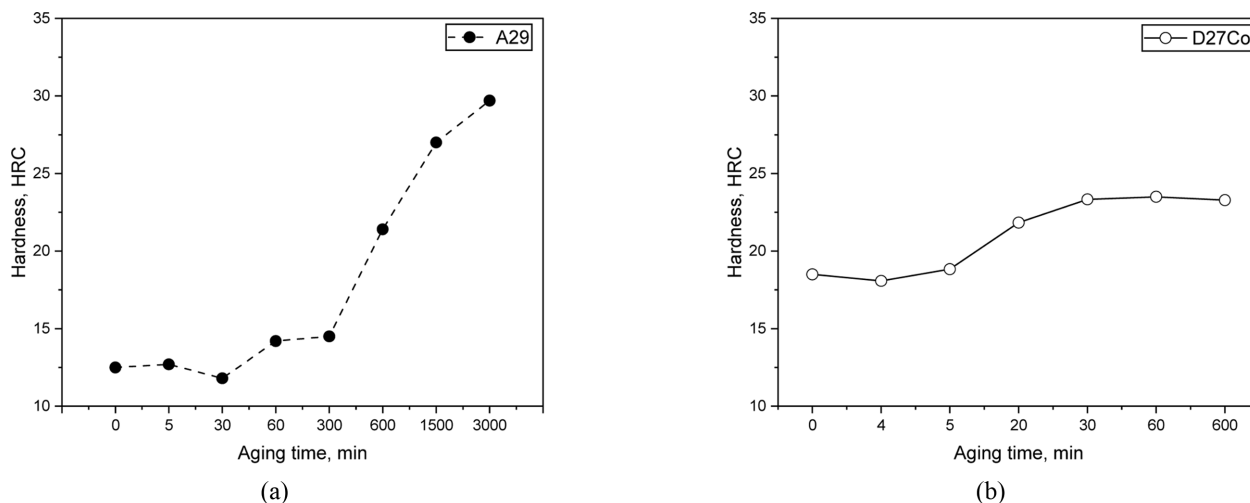


Fig. 3. Effect of aging time on the surface hardness using Rockwell hardness tester: (a) Austenitic A29 alloy and (b) Duplex D27Co alloy

of aging time, and the results are shown in Fig. 3. As shown in the figure, both alloys showed a tendency to increase in hardness with increasing aging time, but the change in hardness varied with aging time. A29 showed a sharp increase in hardness at 600 minutes of aging (Fig. 3a), while D27Co showed a sharp increase in hardness at 30 minutes (Fig. 3b). On the other hand, after the sharp change in hardness, the hardness of A29 continues to increase as the aging time increases, but the hardness of D27Co does not change significantly.

4. Discussion

As described above, it can be seen that the corrosion

and mechanical properties deteriorate significantly with aging time. To determine whether this behavior is essentially related to microstructural changes, XRD was used to analyze the formation of new phases with aging time. Fig. 4 shows the results of XRD measurements of A29, an austenitic stainless steel. Fig. 4a shows the overall data as a function of aging time for A29, and Fig. 4b shows the results of the aging time at which the peak of the precipitation phase was detected, i.e., the peak of the precipitation phase was not detected until the aging time of 1,500 minutes, but the peaks of the sigma and Chi phases were detected at the aging time of 3,000 minutes.

Fig. 5 shows the results of XRD measurements on D27Co, a duplex stainless steel. Fig. 5a shows the overall

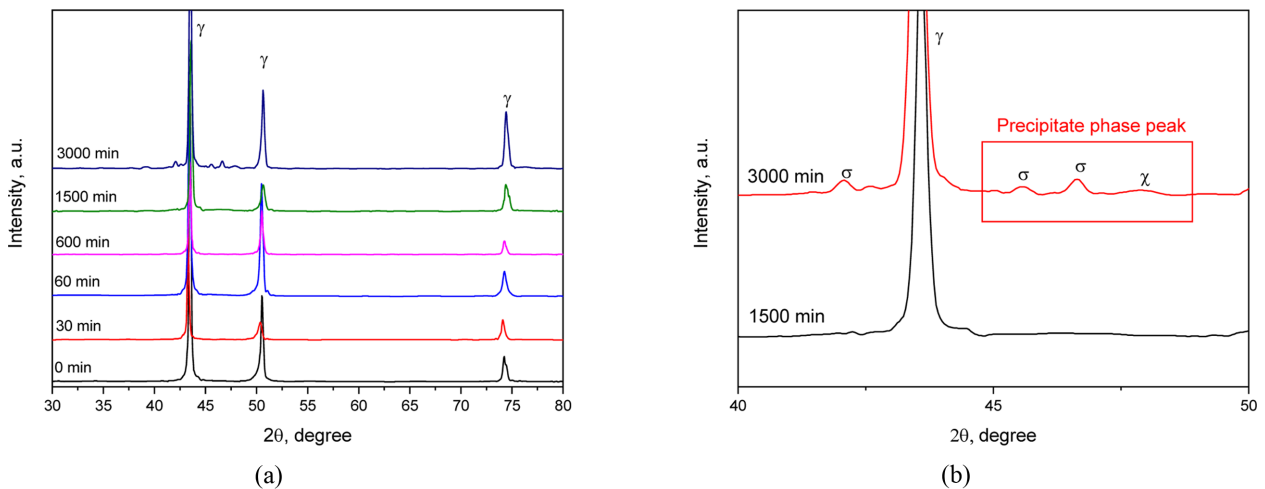


Fig. 4. Effect of aging time on XRD patterns of austenitic A29 alloy

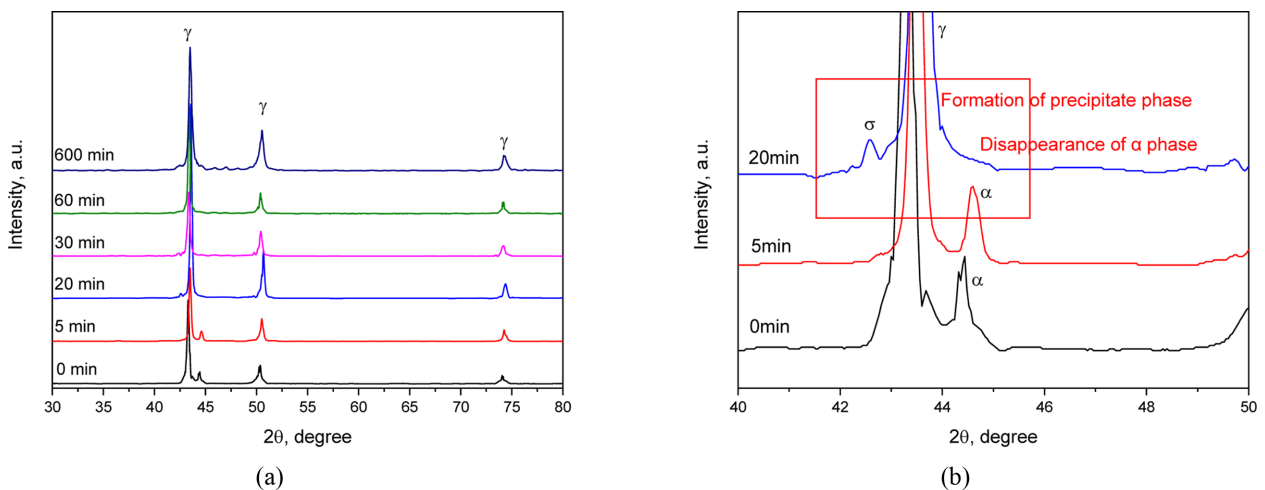


Fig. 5. Effect of aging time on XRD patterns of duplex D27Co alloy

data for D27Co as a function of aging time, while Fig. 5b shows the results for the aging time at which the peak of the precipitated phase was detected. The XRD analysis of D27Co showed that the ferrite disappeared after 20 minutes, while the peak of the sigma phase was detected at the same time.

For both alloys, a peak in the sigma phase was observed with increasing aging time, but the aging time at which the precipitation phase was detected was different.

Fig. 6 shows the effect of aging time on the microstructure of austenitic A29 alloy at 850 °C. Optical microscopy showed little change in microstructure from 0 to 60 minutes of aging time. At an aging time of 300 minutes, precipitated phases were observed at the grain boundaries. At 600 minutes, precipitates were observed inside the grain as well as at the grain boundaries, and at later aging times, precipitates grew inside the grain and at the grain boundaries. In order to observe the microstructure of grains and grain boundaries in detail, the SEM-EBSD unit was used to observe at $\times 5000$. The

results of band contrast and phase color were obtained. From the band contrast observation, it was observed that the thickness of the grain boundary became wider than the boundary thickness of the annealed material until the aging time of 60 minutes. At 300 minutes, a small amount of precipitated phase appeared in the grain as well as in the boundary area. At an aging time of 600 minutes, the growth of the precipitate phase was observed in the boundary region and within the grain, and the precipitate phase continued to grow in the grain boundary region and within the grain at later aging times. Meanwhile, the precipitation phase was analyzed by phase color, where red means BCC crystal structure, blue means FCC crystal structure, and black means sigma phase. From the aging time of 30 min, the sigma phase and the chi phase, which is the BCC crystal structure, were observed in the grain boundary region [37]. At an aging time of 60 min, the sigma and chi phases grew, and at 300 min, the proportion of sigma phase increased rapidly. After 600 min, the proportion of sigma and chi phases increased inside the

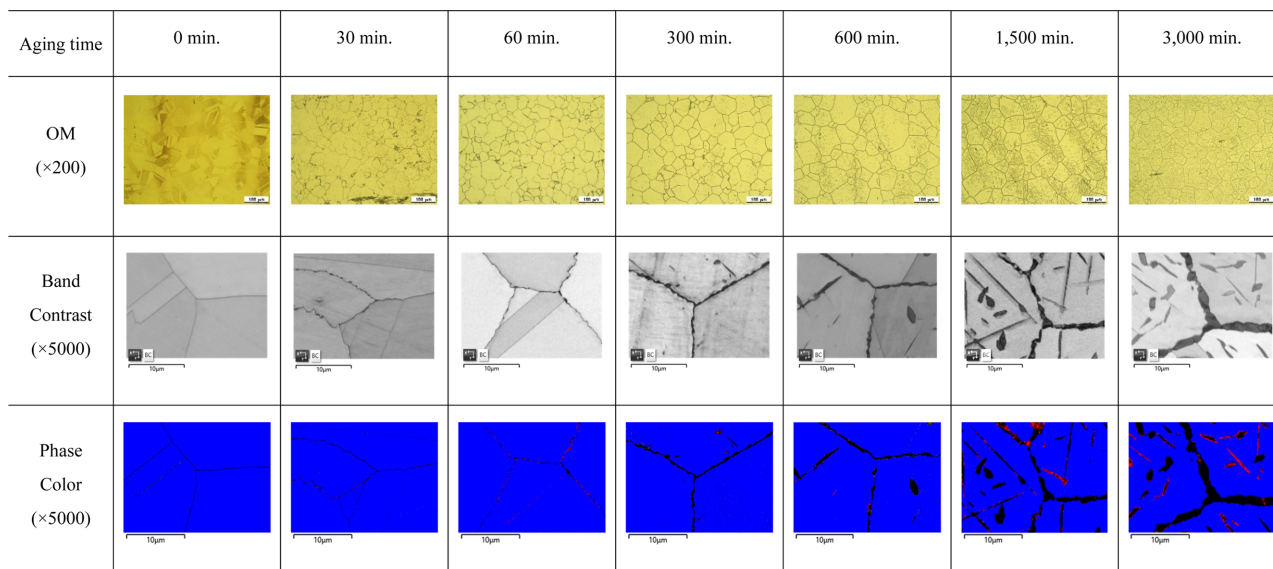


Fig. 6. Effect of aging time on the microstructure of austenitic A29 alloy at 850 °C

Table 2. Material properties and sigma fraction of super austenitic stainless steel A29 by aging

Aging time	0 min.	5 min.	30 min.	60 min.	300 min.	600 min.	1,500 min.	3,000 min.
CPT, °C	80	80	65	55	50	50	45	45
E_{ir} , V	0.88	0.88	0.87	0.9	0	0.003	-0.04	-0.08
Hardness, HRC	12.5	12.7	11.8	14.2	14.5	21.4	27.0	29.7
Sigma in austenite, %	0	0	2.68	2.86	3.02	6.35	10.50	15.06

grains and at the grain boundaries. The amount and properties of the sigma phase as a function of aging time for A29, an austenitic stainless steel, are summarized in Table 2.

Fig. 7 shows the effect of aging time on the microstructure of duplex D27Co alloy at 850 °C. Optical microscopy showed little change in microstructure from 0 to 5 minutes of aging time. At an aging time of 20 minutes, a blackish area was observed within the ferrite structure, which was determined to be a precipitate phase. At 30 minutes of aging time, there was a change to a precipitate phase in the ferrite and a structure presumed to be a second austenite phase, and at later aging times, precipitate phases were also observed in the grain boundaries of the austenitic matrix. In order to observe the microstructure of grains and grain boundaries in detail, the SEM-EBSD unit was used to magnify to $\times 1500$. Band contrast observation showed that there was no significant change in the ferrite and austenite organization until 4 minutes of aging time, and at 5 minutes of aging time, a precipitate phase was observed in the ferrite region. At an aging time

of 20 minutes, the ferrite structure was completely transformed into a precipitate phase, and from this time onward, precipitates were observed not only in the ferrite region but also in the grain boundaries of the austenite base structure. Next, when the precipitate phase was analyzed by phase color, it was found that there was some precipitation of sigma phase inside the ferrite phase at an aging time of 4 minutes, and the proportion of sigma phase gradually increased as the aging time reached 5 minutes. At 20 minutes of aging time, the ferrite had completely transformed into sigma phase, second austenite phase, and Chi phase. In EBSD phase color analysis, the red color indicates a BCC crystal structure, suggesting that this structure may be ferrite or chi phase. Therefore, qualitative magnetic measurements showed no magnetism at all, suggesting that the reddish part of the BCC crystal structure is a chi phase [38]. At an aging time of 30 min, the area of the second austenitic phase increased, and at later times, the sigma phase precipitated and grew in the grain boundaries of the austenitic matrix. The changes in the amount and properties of the sigma

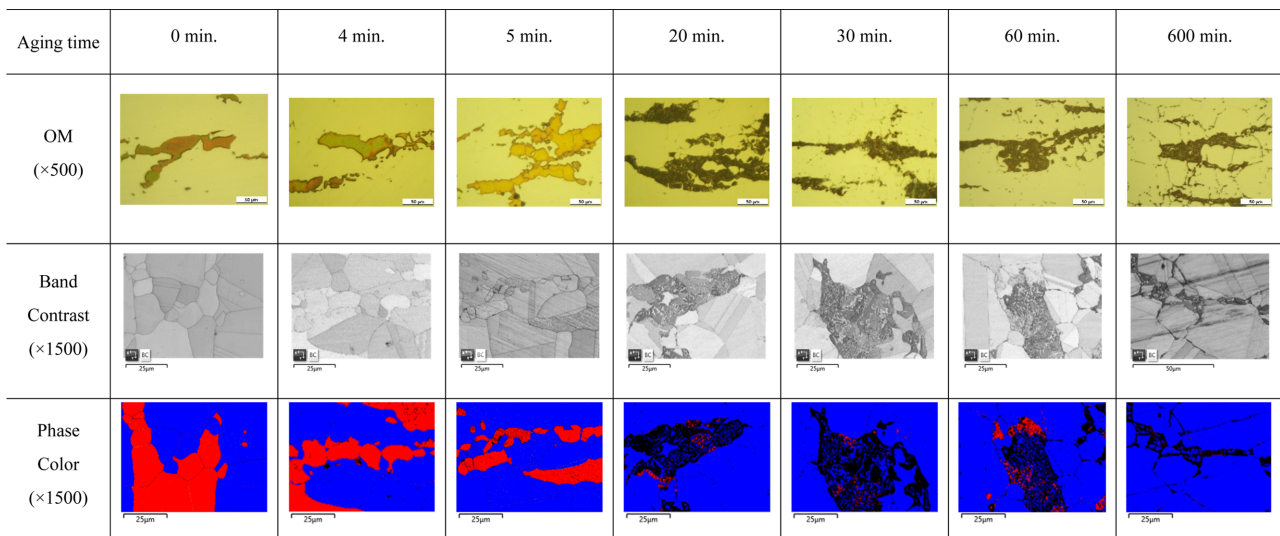


Fig. 7. Effect of aging time on the microstructure of duplex D27Co alloy at 850 °C

Table 3. Material properties and sigma fraction of super duplex stainless steel D27Co by aging

Aging time	0 min.	4 min.	5 min.	20 min.	30 min.	60 min.	600 min.
CPT, °C	85	80	55	40	25	30	25
E_r , V	0.88	0.88	0.88	0.21	-0.056	0.15	0.12
Hardness, HRC	18.5	18.1	18.8	21.8	23.3	23.5	23.3
Sigma in (ferrite + austenite),%	0	0.14	1.63	8.61	16.04	15.55	14.93

phase with aging time for D27Co, a duplex stainless steel, are summarized in Table 3.

Fig. 8 shows the effect of aging time on the properties degradation and sigma formation of Fig. 8a austenitic A29 alloy and Fig. 8b duplex D27Co alloy. This figure is a graphical representation of the data from Table 2

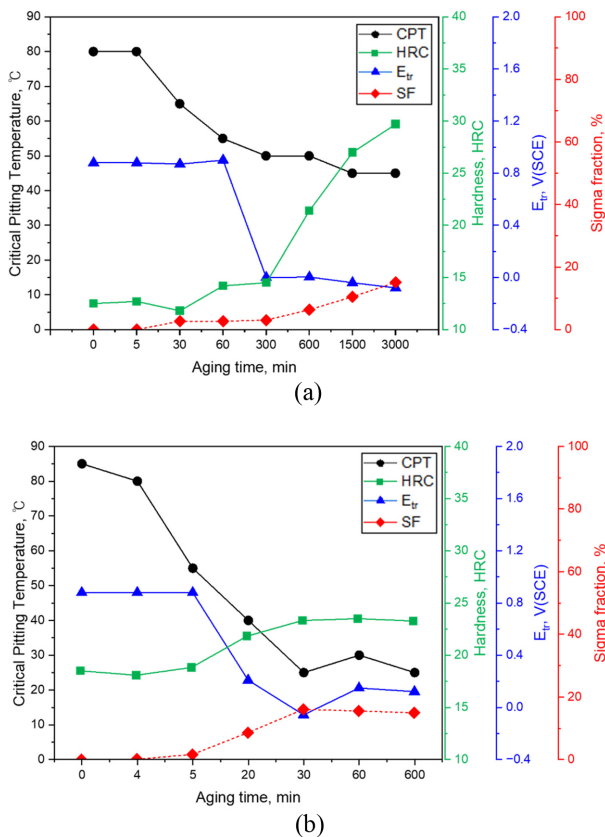


Fig. 8. Effect of aging time on the properties degradation and sigma formation of (a) austenitic A29 alloy and (b) duplex D27Co alloy

and Table 3.

After evaluating the aging properties of A29, an austenitic stainless steel, the critical aging time is as follows. In the corrosion properties, the CPT was found to be 30 minutes, the pitting potential (E_{tr}) was found to be 300 minutes, and the mechanical property, hardness, was found to be 600 minutes. In addition, the fraction of sigma phase increased at aging times of 30 minutes (σ : 2.68%), 300 minutes (σ : 3.02%), and 600 minutes (σ : 6.35%). As such, even at short aging times, small amounts of sigma phase were evaluated to be the most sensitive to degradation of the critical pitting temperature characteristic. Longer aging times and more sigma phases were found to cause a decrease in the pitting potential and an increase in hardness.

After evaluating the aging properties of D27Co, a duplex stainless steel, the critical aging time is as follows. In terms of corrosion properties, CPT was found to be 5 minutes, pitting potential (E_{tr}) was found to be 20 minutes, and hardness, a mechanical property, was found to be 30 minutes. In addition, the fraction of sigma phase increased at aging times of 5 minutes (σ : 1.63%), 20 minutes (σ : 8.61%), and 30 minutes (σ : 16.04%). As such, even at short aging times, small amounts of sigma phase were evaluated to be the most sensitive to degradation of the critical pitting temperature characteristic. Longer aging times resulted in more sigma phase generation, which was associated with a decrease in pitting potential and an increase in hardness.

Table 4 shows the relationship between critical aging time and properties degradation of austenitic and duplex stainless steels. As summarized in Table 4, the CPT of

Table 4. Relationship between critical aging time and properties degradation of austenitic and duplex stainless steels

Properties	Index	Austenitic stainless steel, A29	Duplex stainless steel, D27Co
CPT	Critical aging time, min.	30	5
	Sigma fraction, %	2.68	1.63
	Sigma formation rate, %/min.	0.09	3.1
Ep	Critical aging time, min.	300	20
	Sigma fraction, %	3.02	8.61
	Sigma formation rate, %/min.	0.01	0.43
Hardness	Critical aging time, min.	600	30
	Sigma fraction, %	6.35	16.04
	Sigma formation rate, %/min.	0.01	0.54

D27Co, a duplex stainless steel, degraded at a critical aging time 6 times faster than that of A29, an austenitic stainless steel, and the rate of sigma phase formation was 34.4 times faster. The pitting potential of D27Co, a duplex stainless steel, degraded at an aging time 15 times faster than that of the austenitic A29, and the sigma phase formed 43 times faster. The hardness of D27Co, a duplex stainless steel, increased at an aging time 20 times faster than that of A29, an austenitic stainless steel, and the rate of sigma phase formation was 54 times faster. In other words, both austenitic stainless steels and duplex stainless steels exhibited a similar phenomenon of significant property degradation with increasing aging time, but the critical aging time for property degradation in duplex stainless steels was shorter and the rate of sigma phase formation was faster.

5. Conclusions

In this study, a super austenitic stainless steel with a pitting resistance index of 52.8 and a super duplex stainless steel with an index of 48.7 were evaluated by varying the aging time at 850 °C, and the following conclusions were drawn from the analysis of the critical aging time at which deterioration occurs rapidly.

1) Regardless of austenitic or duplex stainless steels, corrosion properties and hardness degradation occurred with increasing aging time. The fastest degradation rate in the critical pitting temperature was observed and followed by pitting potential and hardness. This was found to be closely related to the fraction of sigma phase.

2) For the critical pitting temperature and pitting potential, the duplex stainless steel degraded at a critical aging time about 6 times and 15 times faster than the austenitic stainless steel, respectively. On the other hand, for the hardness, the duplex stainless steel showed a critical aging time about 20 times faster than the austenitic stainless steel. This trend is due to the faster rate of sigma phase formation in duplex stainless steels.

Acknowledgement

This research was supported by a grant from the 2023-2024 Research funds of Andong National University, and Korea Institute for Advancement of Technology (KIAT)

grant funded by the Korea Government (MOTIE) (P0008458, HRD Program for Industrial Innovation).

References

1. R. R. Maller, Passivation of stainless steel, *Trends in Food Science & Technology*, **9**, 28 (1998). Doi: [https://doi.org/10.1016/S0924-2244\(97\)00004-6](https://doi.org/10.1016/S0924-2244(97)00004-6)
2. A. H. Tuthill and R. E. Avery, Specifying stainless steel surface treatments, *Advanced Materials & Processes*, **142**, 34 (1992).
3. K. Sotoodeh, Analysis and improvement of material selection for process piping system in offshore industry, *American Journal of Mechanical Engineering*, **6**, 17 (2018). Doi: <https://doi.org/10.12691/ajme-6-1-3>
4. E. Messinese, L. Casanova, L. Paterlini, F. Capelli, F. Bolzoni, M. Ormellese, A. Brenna, A comprehensive investigation on the effects of surface finishing on the resistance of stainless steel to localized corrosion, *Metals*, **12**, 1751 (2022). Doi: <https://doi.org/10.3390/met12101751>
5. D. Kim, W. Chung, B. H. Shin, Effects of the volume fraction of the secondary phase after solution annealing on electrochemical properties of super duplex stainless steel UNS S32750, *Metals*, **13**, 957 (2023). Doi: <https://doi.org/10.3390/met13050957>
6. Y. Das, J. Liu, H. Ehteshami, J. Odqvist, N. H. Pettersson, S. Wessman, S. King, P. Hedström, Quantitative nanostructure and hardness evolution in duplex stainless steels: under real low-temperature service conditions, *Metallurgical and Materials Transactions A*, **53**, 723 (2022). Doi: <https://doi.org/10.1007/s11661-021-06547-4>
7. G. Kim, S. H. Shin, B. Hwang, Machine learning approach for prediction of hydrogen environment embrittlement in austenitic steels, *Materials Research and Technology*, **19**, 2794 (2022). Doi: <https://doi.org/10.1016/j.jmrt.2022.06.046>
8. S. Y. Won, G. B. Kim, Y. R. Yoo, S. H. Choi, and Y. S. Kim, Intergranular corrosion behavior of medium and low carbon austenitic stainless steel, *Corrosion Science and Technology*, **21**, 230 (2022). Doi: <https://doi.org/10.14773/cst.2022.21.3.230>
9. N. L. Isern, H. L. Luque, I. L. Jiménez, M. V. Biezma, Identification of sigma and chi phases in duplex stainless steels, *Materials Characterization*, **112**, 20 (2016). Doi: <https://doi.org/10.1016/j.matchar.2015.12.004>
10. K. H. Lo, C. H. Shek, J. K. L. Lai, Recent developments in

- stainless steels, *Materials Science and Engineering R*, **65**, 39 (2009). Doi: <https://doi.org/10.1016/j.mser.2009.03.001>
11. A. F. Padilha, P. R. Rios, Decomposition of Austenite in Austenitic Stainless Steels, *ISIJ International*, **42**, 325 (2002). Doi: <https://doi.org/10.2355/isijinternational.42.325>
 12. T. H. Chen, J. R. Yang, Effects of solution treatment and continuous cooling on σ -phase precipitation in a 2205 duplex stainless steel, *Materials Science and Engineering A*, **311**, 28 (2001). Doi: [https://doi.org/10.1016/s0921-5093\(01\)00911-x](https://doi.org/10.1016/s0921-5093(01)00911-x)
 13. L. Duprez, B. C. D. Cooman, N. Akdut, Redistribution of the substitutional elements during σ and χ phase formation in a duplex stainless steel, *Steel Research*, **72**, 311 (2001). Doi: <https://doi.org/10.1002/srin.200100123>
 14. D. M. E. Villanueva, F. C. P. Junior, R. L. Plaut, A. F. Padilha, Comparative study on sigma phase precipitation of three types of stainless steels: austenitic, super ferritic and duplex, *Materials Science and Technology*, **22**, 1098 (2006). Doi: <https://doi.org/10.1179/174328406x109230>
 15. D. Wasnik, G. K. Dey, V. Kain, I. Samajdar, Precipitation stages in a 316L austenitic stainless steel, *Scripta Materialia*, **49**, 135 (2003). Doi: [https://doi.org/10.1016/s1359-6462\(03\)00220-3](https://doi.org/10.1016/s1359-6462(03)00220-3)
 16. M. Schwind, J. Källqvist, J. O. Nilsson, J. Ågren, H. O. Andrén, σ -phase precipitation in stabilized austenitic stainless steels, *Acta Materialia*, **48**, 2473 (2000). Doi: [https://doi.org/10.1016/s1359-6454\(00\)00069-0](https://doi.org/10.1016/s1359-6454(00)00069-0)
 17. H. U. Hong, B. S. Rho, S. W. Nam, Correlation of the $M_{23}C_6$ precipitation morphology with grain boundary characteristics in austenitic stainless steel, *Materials Science and Engineering A*, **318**, 285 (2001). Doi: [https://doi.org/10.1016/s0921-5093\(01\)01254-0](https://doi.org/10.1016/s0921-5093(01)01254-0)
 18. S. Zhang, H. Li, Z. Jiang, B. Zhang, Z. Li, J. Wu, S. Fan, H. Feng, H. Zhu, Effects of Cr and Mo on precipitation behavior and associated intergranular corrosion susceptibility of super austenitic stainless steel S32654, *Materials Characterization*, **152**, 141 (2019). Doi: <https://doi.org/10.1016/j.matchar.2019.04.010>
 19. J. Xiao, Y. Zhang, W. Zhang, A. Zhao, Precipitation mechanism of σ phase in S32654 super austenitic stainless steel, *Materials Letter*, **349**, 134834 (2023). Doi: <https://doi.org/10.1016/j.matlet.2023.134834>
 20. J. K. Kim, Y. H. Kim, J. S. Lee, K. Y. Kim, Effect of chromium content on intergranular corrosion and precipitation of Ti-stabilized ferritic stainless steels, *Corrosion Science*, **52**, 1847 (2010). Doi: <https://doi.org/10.1016/j.corsci.2010.01.037>
 21. Y. W. Chai, K. Kato, C. Yabu, S. Ishikawa, Y. Kimura, Disconnections and Laves (C14) precipitation in high-Cr ferritic stainless steels, *Acta Materialia*, **198**, 230 (2020). Doi: <https://doi.org/10.1016/j.actamat.2020.08.006>
 22. M. P. Sello, W. E. Stumpf, Laves phase precipitation and its transformation kinetics in the ferritic stainless steel type AISI 441, *Materials Science and Engineering A*, **528**, 1840 (2011). Doi: <https://doi.org/10.1016/j.msea.2010.09.090>
 23. H. P. Qu, Y. P. Lang, H. T. Chen, F. Rong, X. F. Kang, C. Q. Yang, H. B. Qin, The effect of precipitation on microstructure, mechanic properties and corrosion resistance of two UNS S44660 ferritic stainless steels, *Materials Science and Engineering A*, **534**, 436 (2012). Doi: <https://doi.org/10.1016/j.msea.2011.11.091>
 24. D. H. Kim, K. C. Kim, J. H. Park, W. Chung, B. H. Shin, Microstructure and corrosion performance of high-entropy alloy and austenite and super duplex stainless steels in 3.5% NaCl solution, *International Journal of Electrochemical Science*, **18**, 100074 (2023). Doi: <https://doi.org/10.1016/j.ijeoes.2023.100074>
 25. K. Chan, S. Tjong, Effect of secondary phase precipitation on the corrosion behavior of duplex stainless steels, *Materials*, **7**, 5268 (2014). Doi: <https://doi.org/10.3390/ma7075268>
 26. H. Sieurin, R. Sandström, Sigma phase precipitation in duplex stainless steel 2205, *Materials Science and Engineering A*, **444**, 271 (2007). Doi: <https://doi.org/10.1016/j.msea.2006.08.107>
 27. C. S. Huang, C. C. Shih, Effects of nitrogen and high temperature aging on σ phase precipitation of duplex stainless steel, *Materials Science and Engineering A*, **402**, 66 (2005). Doi: <https://doi.org/10.1016/j.msea.2005.03.111>
 28. A. J. Ramirez, J. C. Lippold, S. D. Brandi, The relationship between chromium nitride and secondary austenite precipitation in duplex stainless steels, *Metallurgical and Materials Transactions A*, **34**, 157 (2003). Doi: <https://doi.org/10.1007/s11661-003-0304-9>
 29. X. Huang, D. Wang, Y. Yang, Effect of precipitation on intergranular corrosion resistance of 430 ferritic stainless steel, *Journal of Iron and Steel Research International*, **22**, 1062 (2015). Doi: [https://doi.org/10.1016/s1006-706x\(15\)30113-8](https://doi.org/10.1016/s1006-706x(15)30113-8)
 30. S. Zhang, H. Li, Z. Jiang, Z. Li, J. Wu, B. Zhang, F. Duan, H. Feng, H. Zhu, Influence of N on precipitation behavior, associated corrosion and mechanical properties of super austenitic stainless steel S32654, *Journal of Materials Science & Technology*, **42**, 143 (2020). Doi: <https://doi.org/10.1016/j.jmst.2020.01.001>

- <https://doi.org/10.1016/j.jmst.2019.10.011>
31. K. T. Kim, S. B. Um, Y. S. Kim, Effect of heat treatment on the corrosion properties of seamless 304L stainless steel pipe, *Corrosion Science and Technology*, **16**, 305 (2017). Doi: <https://doi.org/10.14773/cst.2017.16.6.305>
 32. Y. T. Jeon, Y. S. Kim, Y. S. Park, W. S. Ryu, J. H. Hong, Influences of aging heat treatment on the microstructure, mechanical properties, and corrosion resistance of Fe - Cr - Mn type stainless steels, *Corrosion Science and Technology*, **30**, 61 (2001).
 33. Z. Y. Liu, F. Gao, L. Z. Jiang, G. D. Wang, The correlation between yielding behavior and precipitation in ultra purified ferritic stainless steels, *Materials Science and Engineering A*, **527**, 3800 (2010). Doi: <https://doi.org/10.1016/j.msea.2010.03.047>
 34. Y. S. Kim, D. B. Mitton, R. M. Latanision, Corrosion resistance of stainless steels in chloride containing supercritical water oxidation system, *Korean Journal of Chemical Engineering*, **17**, 58 (2000). Doi: <https://doi.org/10.1007/bf02789254>
 35. K. G. Kim, H. Y. Chang, Y. S. Kim, Effect of thermal history on pitting corrosion of high nitrogen and low molybdenum stainless steels, *Corrosion Science and Technology*, **2**, 2, 75 (2003).
 36. ASTM G48, Standard test methods for pitting and crevice corrosion resistance of stainless steels and related alloys by use of ferric chloride solution, ASTM (2003).
 37. A. D. Warren, I. J. Griffiths, P. E. J. Flewitt, Precipitation within localised chromium-enriched regions in a Type 316H austenitic stainless steel, *Journal of Materials Science*, **53**, 6183 (2018). Doi: <https://doi.org/10.1007/s10853-017-1748-4>
 38. D. M. Escriba, E. M. Morris, R. L. Plaut, A. F. Padilha, Chi-phase precipitation in a duplex stainless steel, *Materials Characterization*, **60**, 1214 (2009). Doi: <https://doi.org/10.1016/j.matchar.2009.04.013>